Functionalized Silica Nanoparticles by Nanometallic Ag Decoration for Optical Sensing of Organic Molecule

Ren-Der Jean,[†] Kuo-Chuang Chiu,[‡] Tsung-Han Chen,[†] Chun-Hua Chen,*[,†] and Dean-Mo Liu*[,†]

Department of Materials Science and Engineering, National Chiao Tung University, Hsinchu, Taiwan 300, ROC, and Material and Chemical Research Laboratories, Industrial Technology Research Institute, Hsinchu, Taiwan 310, ROC

Received: July 5, 2010; Revised Manuscript Received: August 11, 2010

Sensing technologies based on metallic nanoparticles, known as Ag, Au, and so on, have raised enormous interest for their extraordinary sensing resolution and sensitivity to analytes of chemical or biological importance under optical detection have received wide attention in recent decades. Currently, a discrete nanoparticle in a free-standing form, either being organically or biologically modified on the nanoparticle surface, on a given substrate surface region has been employed for photosensing purpose. However, metallic nanoparticles suffering from physical and chemical instability such as oxidation, interparticle coupling, agglomeration, and so on during the processing stages may render undesirable outcomes, which further results in poorer performance than the theoretical expectation. Here we propose a facile and elegant concept to prepare an Ag-decorated silica nanoparticle (hereinafter termed core−shell SiO_2@Ag nanosphere) based on the modified Stöber method. The Ag nanoparticles with an average size controlled at about 1, 3, and 5 nm deposited over the surface of the silica nanocarrier were well separated, making the resulting SiO_2@Ag nanospheres. The nanospheres showed physically and optically stable surface plasmon resonance spectra and also demonstrated a relatively high Ag-sized dependent sensitivity to ppb level for the detection of analyte molecule, that is, melamine. Theoretical model fitting has been well managed to correlate the optical behavior of the nanosensors, and the outcomes strongly indicated a promising potential of the Ag-decorated SiO_2 core−shell nanospheres for sensory applications.

1. Introduction

The design of core−shell nanoparticles with various functionalities for advanced applications has become one of the most exciting movements in the development of cross-disciplinary nanotechnology. The core−shell nanoobjects represent one of the most interesting areas of material science because of their tailored properties that can be optimized with respect to constituting merits. Among those disciplines, utilization for sensing analytes of chemical or biological nature has become a major advance in the field.[1,2] Nanosized noble metal shell deposited on nanoparticle core has shown outstanding surface plasmon resonance in the visible range. The surface plasmon resonance (SPR) peak also appears if such a metal is deposited onto dielectric particle such as silica either as a thin shell or particle assembly. Peak position of the plasmon resonance depends on thr core-to-shell ratio and is also sensitive to the surrounding medium.[3,4] In the meantime, it was also observed that the peak wavelength showed a dependence on particle size, particle shape, and interparticle coupling.[5−7]

Silica has long been employed as a promising candidate to prepare core−shell nanoobjects, either as shell or core materials. For instance, Liz-Marzán et al.[8] prepared metal−silica core−shell nanoparticles by using a silane coupling agent to form silanol groups anchored on the metal surface to give a chemical link with the silica surface. They showed that through the silanol bonds, th esilica shell has enhanced colloidal and chemical stability of resulting core−shell nanoparticles in a given medium; it also controlled the distance between core particles within assemblies through shell thickness. Kobayashi et al.[1] reported in a recent report silica coating onto silver nanoparticles via a modified Stöber method using dimethylamine as a catalyst to obtain silica coating. Yin et al.[2] successfully prepared silica-coated silver coaxial nanocable simply through hydrolysis and condensation of tetraethylorthosilicate (TEOS) in ethanol. The resulting silver/silica nanocables showed a well-controlled sheath thickness in the range of 2−100 nm. The lengths of these nanocables could be up to 50 μm. Direct coating of PVP-stabilized metal nanoparticles using TEOS has also demonstrated.[3] From those reports, a resulting change in conductivity and optical properties has been experimentally verified when the core particles were covered with a thin silica shell. Besides, silica NPs have emerged as a suitable matrix rather than a coating medium because of their surface functionality, following bioconjugation with a number of active molecules for such as monitoring and biomarking in biomedical sectors. Oxide−metal core−shell structures with gold or silver nanoparticle shells on a silica or titania core have received increasing attention over the years for advanced applications,[4−6] including chemical sensors, biosensors, labeling, and so on. However, the metallic shells were virtually constructed by a dense and close packing of either silver or gold nanoparticles; although a fairly powerful sensing resolution can be achieved, a strong interparticle coupling effect may arise, which further reduces sensing resolution and sensitivity.

Therefore, when developing a nanoparticle-based sensing device, it may be an ideal design if the surface area of a given nanoparticle and its surface-anchored bioactive molecules can

* Corresponding authors. E-mail: deanmo_liu@yahoo.ca (D.-M.L.), chunhuachen@mail.nctu.edu.tw (C.-H.C.).
[†] National Chiao Tung University.
[‡] Industrial Technology Research Institute.

10.1021/jp106185m © 2010 American Chemical Society
Published on Web 08/26/2010

be fully available for analyte detection. This requires a design to which sensing nanoparticles should be stably separated in a given medium or onto a substrate. Although functionalized nanoparticles including silver, gold, quantum dots, Eu_2O_3, and so on have been extensively employed to enhance sensory power because of surface-enhanced plasmon resonance, a potential of forming aggregates or a reduction of exposed surface of a given nanoparticle-based sensor, either in a solution type or aggregated onto a substrate, was virtually inevitable because of interparticle interactions that reduce or alter the resolution or precision of SPR spectrum as a result of coupling. To this point, a risk of unexpected measuring errors may surely develop, giving rise to unreliable data interpretation. The SPR-induced optical absorption peaks observed in metallic nanoparticles, especially in the noble metals, is of great interest for both fundamental and practical reasons.[9−12] The spectral position, half width, and intensity of the optical absorption of the metallic nanoparticles are the comprehensive results of intrinsic properties, for example, composition, size, morphology, and aggregated geometry of the nanoparticles and also extrinsic influence from the surrounding medium as well as the carrier or substrate materials. Different models can be used to describe these optical dependencies.

Here we employed a nanosized silica as a core substrate and particularly as a spacer via a modified Stöber process without using any coupling agents following a complexation of silver ions with the presence of ammonia in water/ethanol solutions to synthesize silver-coated silica nanospheres. The population and size of the silver nanoparticle on the silica nanomatrix were precisely controlled for spectral analysis, whereas an organic molecule, melamine, was employed as a model analyte adsorbed onto the silver surface. Recently, melamine detection became an important issue because of its illegal existence in many food productions. Well-dispersed Au and Ag nanoparticles (generally >10 nm) with or without surface modification have been applied to detect melamine concentration with colorimetric analyses. These methods are all based on the principle that the interspacing between nanoparticles is rather sensitive to the melamine concentration and thus change the absorption ratio of two specific wavelengths in the SPR spectra.[13−15] In contrast with the above proposed methods using varying nanoparticle spacing, we newly designed sensors with a constant nanoparticle spacing by depositing extremely small Ag nanoparticles on SiO_2 nanocarriers, that is, SiO_2@Ag.

It is expected that the sparingly distributed silver nanoparticles on the silica matrix permit a stable and improved resolution/precision of the emitting spectrum for sensing small organic molecules over prolonged durations. In the meantime, the formed silver nanoparticles allow us to keep from undesirable aggregation because they were well anchored and separated with the silica spacer between the nanospheres. To illustrate further the advantage of employing a silica spacer, a liquid-type sensing prototype was employed, that is, in a form of liquid suspension, where the surface area of the anchored nanosilver particles can be fully utilized for the purpose, except for the small regions contacted with the underlying silica nanomatrix. It is expected that such a nanoparticulate core−shell design provides great advantages of sensing stability, accuracy, and sensitivity.

2. Experimental Method

2.1. Preparation of the Core−Shell Nanoparticles. All chemicals used were Aldrich grade, including TEOS (98%), silver nitrate ($AgNO_3$), ethanol (C_2H_5OH, 98%), ammonia, and sodium hydroxide (NaOH) (Sigma-Aldrich, St. Louis, MO).

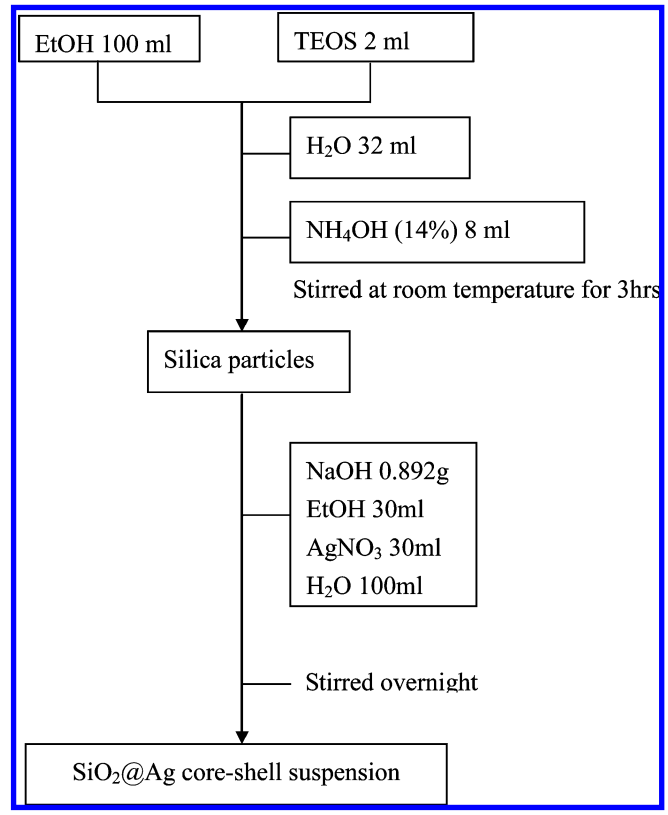

Figure 1. Flowchart of the experimental procedure.

Deionized (DI) water was used in all experiments. All chemicals were used as purchased without any purification.

The method used to prepare the silver shell−silica core nanospheres is based on a Stöber synthesis method modified with the addition of colloidal silver nanoparticles. In a single reaction vessel, initially, we added the follow reagents: 2 mL of TEOS for synthesis, 100 mL of absolute ethanol, 8 mL of ammonia 14%, and 10 mL of DI water; all reactants were mixed by stirring at 300 rpm with a magnetic stir bar at different temperatures from 25 to 75 °C. Then, the solution pH was controlled in the range of 10.5 to 11.2. Then, 0.892 g NaOH, 30 mL of ethanol, 30 mL of silver nitrate, and 100 mL of DI water were added to form a final solution at a pH controlled over a range of 9.2 to 10. The flowchart of the core−shell nanoparticle preparation is shown in Figure 1. The morphology and particle size of the silica and silver were analyzed using a JEOL JEM-2100F field emission transmission electron microscopy (FE-TEM) operated at 200 kV. The UV−vis absorption spectra were performed on a Thermo Scientific Evolution 600 spectrometer.

2.2. Sensing Measurement. The prepared SiO_2@Ag core−shell nanoparticles were suspended in DI water−ethanol solution, followed by the use of UV−vis absorption spectroscopy (Evolution 600, Thermo Scientific) for sensing measurement. The targeted analyte of melamine (Aldrich, 99%) was dissolved in DI water, and standard aqueous solutions with concentration of 0.1, 1, 10, 100, and 1000 ppm were first characterized to establish a calibration profile for a subsequent sensing measurement. For optical characterization, the UV−vis absorption spectra ranging from 300 to 1100 nm were repeatedly recorded after 120 μL of the 1 nm SiO_2@Ag, or 40 μL of the 3 and 5 nm SiO_2@Ag colloidal suspension was added to 1 mL of melamine solutions.

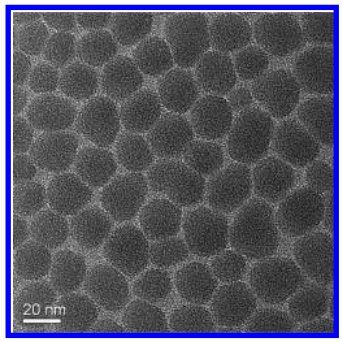

Figure 2. TEM images showing nearly 20 nm bare silica particles.

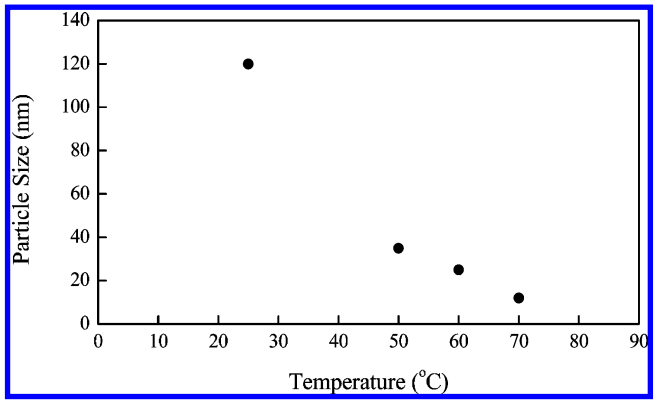

Figure 3. Average particle size of silica depends on the synthesis temperature.

3. Results and Discussion

3.1. Silica Nanoparticle Formation. Figure 2 shows the TEM images of bare silica nanoparticles, where a near spherical appearance with dense surface and relatively homogeneous distribution was observed. The nanoparticle size decreased from 120 nm to ~15 nm as the synthesis temperature increased from 25 to 75 °C. This temperature-dependent size reduction should be stemming from a higher nucleation rate of the silica in the solution when solution temperature was increased. As a result, more nuclei evolved, leading to smaller crystal development. In the meantime, a corresponding change of nanoparticle geometry from sphere to polygon was also detected (Figure 3). The evolution of polygonal geometry of the silica nanoparticles may be a result of unmatured crystal development upon rapid nucleation−growth forming kinetics at higher temperatures. However, in comparison with those silica−metal core−shell nanoparticles reported in literature, the size of the silica nanoparticles (or termed carrier) of the present work is much smaller, by about 10 times, than that of those silica particles previously reported, which were typically on the order of 200 nm in diameter.[7,16] One advantage for the present smaller silica carriers is the ability to carry more silver nanoparticles in a given unit volume of the carriers. To this point, even a lower concentration of the resulting silica−silver nanospheres is then capable of providing higher surface availability of the deposited silver nanoparticles exposed to the environment for a reliable detection of organic molecules with higher sensitivity, stability, and accuracy.

3.2. Silver-Decorated Silica Core−Shell Nanoparticle. The structural morphology of the silver-decorated silica (SiO_2@Ag) core−shell nanospheres is representatively illustrated in Figure 4. The silica carrier has an average size of 20 nm in diameter, and those silver nanoparticles deposited on the silica surface have an average size of 3 nm in size. An average distance between adjacent silver nanoparticles has a separation of 6.8

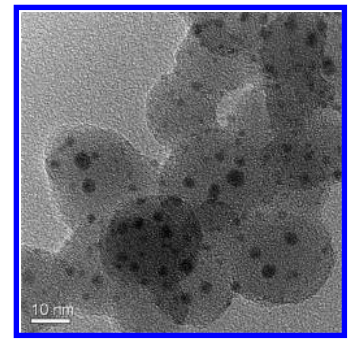

Figure 4. One representative TEM image showing nanoshells of ~3 nm silver nanoparticles on silica carriers.

nm, about 2.3 times the silver particle size. This separation ensures minimal interparticle coupling that may arise to interfering measured accuracy a spectral variation due to adsorption of organic analytes onto the silver nanodetectors.

Upon silver nanoparticle synthesis, the particle size and the population of the silver on the silica carriers can be varied depending on the synthesis conditions. For the former, a decrease in size of the silver was observed from an average of 5 to ~1 nm when the solution pH was finely tuned from 9.2 to 10 by increasing addition of sodium hydroxide. Such a variation in silver particle size may be resulting from an accelerated precipitation of the silver ions when it was approaching the increasingly negatively charged silica carriers as solution pH was increased. According to the synthesis scheme, the OH^- ions were adsorbed on the silica surface and the density of the OH^- adsorption may increase with increasing solution pH, that is, with increasing NaOH addition. The $AgNO_3$ added to the solution elaborated a redox reaction at the sites of OH^- on the silica surface to form Ag metal. The overall reactions can be grossly described by following eqs 1 and 2

$$SiO_2 + H_2O + NaOH \rightarrow SiO_2(OH)^- + H_2O + Na^+ \quad (1)$$

$$Ag^+ + (NO3)^- + SiO_2(OH)^- + H_2O + Na^+ \rightarrow Ag\cdots SiO_2 + 2H_2O + Na(NO_3) \quad (2)$$

In eq 1, the presence of hydroxyl groups promotes a subsequent adsorption toward the silica surface, making the silica nanocarriers more negatively charged, and in consequence, the positively charged silver ions allow chemical attachment to the silica surface (eq 2), where the notation of $Ag\cdots SiO_2$ in eq 2 represents the resulting Ag nanoparticles formation and deposits in situ on the surface of the silica carriers. The adsorption of OH^- ions on the surface takes place through electrostatic interaction with the negatively charged silica surface, as schematically shown in Figure 5. Once the particle surface was chemically modified, the addition of a silver salt lead to a selective redox reaction on the silica surface, forming metallic Ag nanoparticles. The formation of metallic silver upon the addition of Ag ions was also reflected in a color change to dark yellow. It is reasonably to believe that pH increase gradually caused an increase in the amount of OH^- ions, leading to more Ag nanoparticles to nucleate and grow in a given surface area. The decrease in size of the silver nanoparticles was observed from an average of 5 to ~1 nm when the solution pH was increased, which further implied that OH^- ions adsorbed

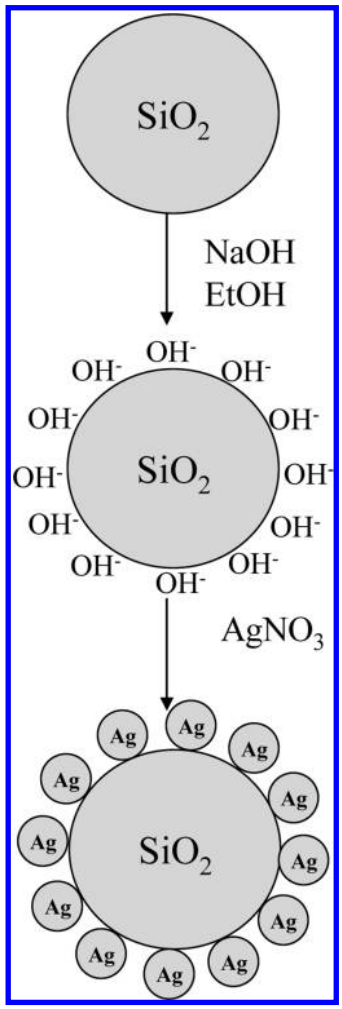

Figure 5. Sketch of surface reactions produced during the formation of silver nanoparticles on the silica carriers.

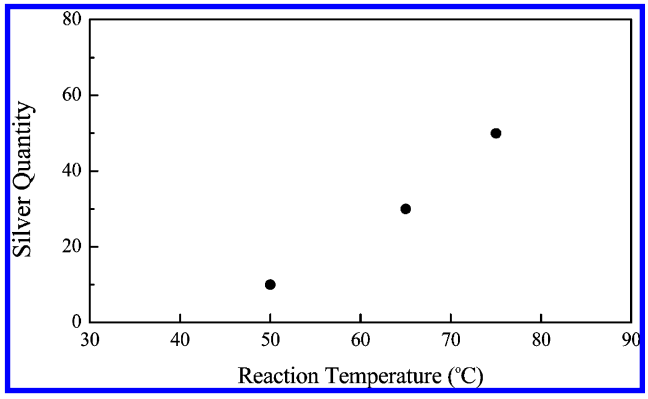

Figure 6. Quantity of silver nanoparticles deposited on the silica carriers at various synthesis temperatures.

on the silica surface were acting as nucleation sites. The more the OH^- anchored to the silica surface, the smaller the size of the Ag nanoparticles evolved.

The quantity of the silver nanoparticle deposited onto the silica carriers was found to increase linearly with synthesis temperature, from 50, 65, to 75 °C, as shown in Figure 6, corresponding to an average of ca.∼10, ∼32, and ∼50 silver nanoparticles per silica carrier, respectively. Figure 7a,b shows the ones with ca.∼10 and ∼50 silver nanoparticles on the silica carriers at a synthesis temperature of 50 and 75 °C, respectively, where the particle size of the silver is ∼3 nm on average. The

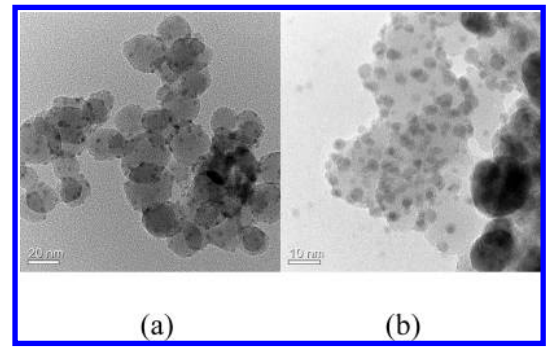

Figure 7. Silver nanoparticles formed and deposited in situ on the silica carriers with a population of ca. (a) ∼10 and (b) ∼50 silver nanoparticles prepared at a synthesis temperature of 50 and 75 °C, respectively.

size of silver nanoparticles is closely resembled to that aforementioned, which is solution pH-dependent but less dependent on the synthesis temperature. This finding suggests a fine-tune of the size and population of the silver nanoparticles onto a given silica nanocarrier that can be easily achievable under the current experimental protocol.

3.3. Optical Properties of SiO_2@Ag Core−Shell Nanoparticles. Figure 8 shows the experimental UV−vis absorption spectra of 1, 3, and 5 nm Ag nanoparticles on SiO_2 nanocarriers and corresponding numerical calculations. The only broad absorption peaks observed around 425 nm for these three SiO_2@Ag nanocarriers are very similar to the SPR of well-suspended Ag nanoparticles in liquid or embedded in silica, as reported elsewhere.[17] As the size of the Ag nanoparticles decreased, the increased surface-to-volume ratio gave rise to electron scattering and broadened the SPR.

According to the TEM images shown in Figure 4, the discrete Ag nanoparticles deposited on SiO_2 nanocarriers display spherical morphology, and the spacing between neighboring nanoparticles is larger than at least one diameter in average. Pellegrini's simulation clearly indicated the less difference in SPR between an isolated Ag nanoparticle and its dimers with an interparticle spacing larger than one diameter.[18] It is thus reasonable to ignore the interaction effects between Ag nanoparticles on SPR for the following simulation work.

First, we simply treated the SiO_2@Ag core−shell nanoparticles as isolated Ag nanoparticles without SiO_2 nanocarriers for the model construction because the UV−vis absorption spectrum of SiO_2 seems featureless, as can be seen in Figure 8. Therefore, the optical absorption spectra can be calculated using the classic Mie theory, which is virtually valid only for isolated spherical particles.[19] Because the present Ag nanoparticle size is much smaller than the mean free path of conduction electrons in the Ag bulk (39 nm),[20] the complex dielectric function of Ag bulk used for Mie calculation should be modified with the Drude model for Ag nanoparticles.[21] Some other optical constants needed were taken from the literature.[22] The calculated spectra (not shown here) fit the experimental spectra well, excluding a slight departure at the very beginning around 300 nm, which should arise from the presumed absence of SiO_2 nanocarriers in our simplified model.

To treat the Ag nanoparticles together with SiO_2 nanocarriers, some theoretical approaches have been developed under the framework of generalized multiparticle Mie theory (GMM),[18] discrete dipole approximation (DDA),[23] or effective medium theory (EMT).[24] For these calculations, structural parameters such as size/thickness, relative position, and volume fraction are required to construct an ideal theoretical model and are input

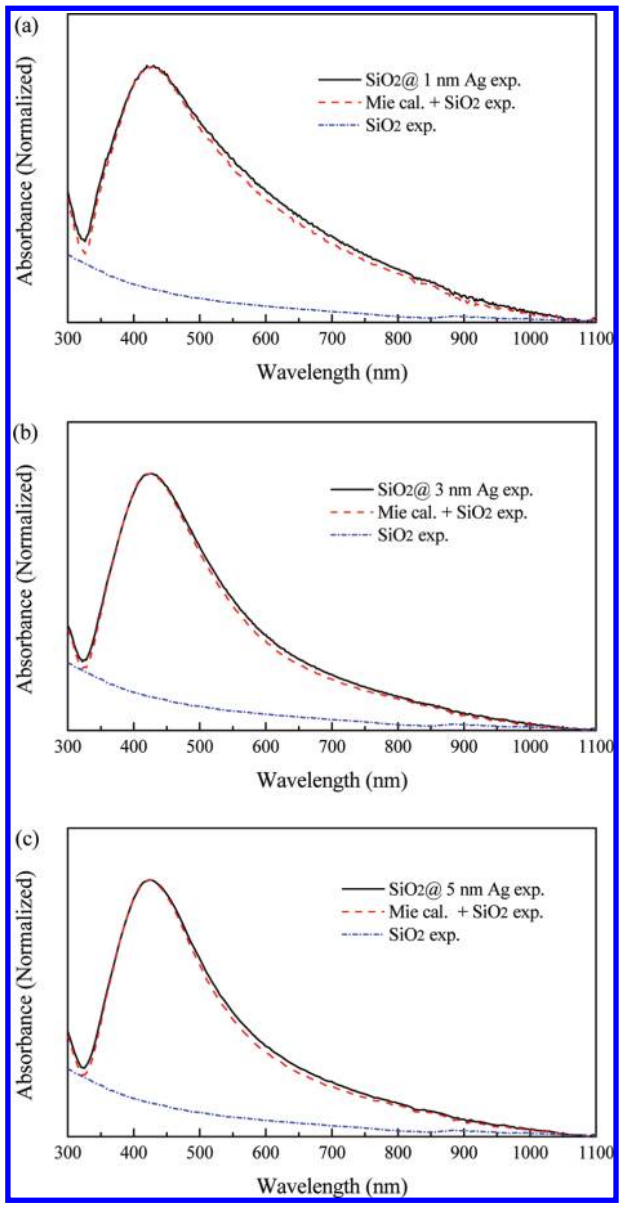

Figure 8. Comparison between the experimental (solid line) and simulated (dashed line) extinction spectra for (a) 1, (b) 3, and (c) 5 nm Ag nanoparticles on the SiO_2 supporters. Experimental absorption spectrum of water with dispersed SiO_2 nanocarriers is comparatively displayed (dot line).

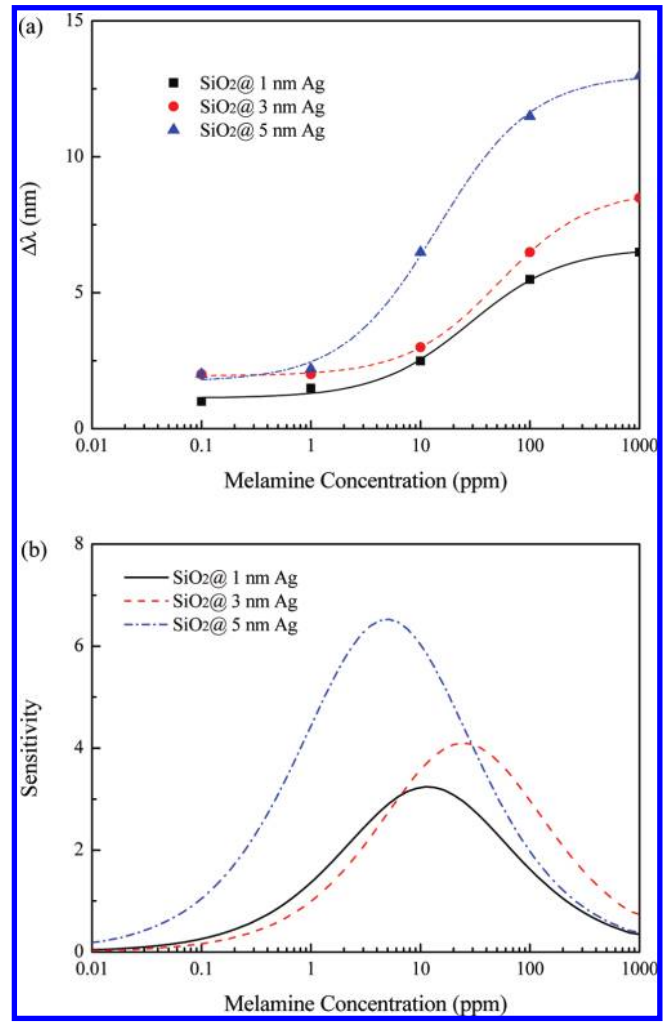

Figure 9. (a) Melamine-concentration-dependent SPR peak shifts for the three Ag nanoparticle sizes. (b) Differential plots derived from part a.

as constants. However, for a real specimen, the experimental spectra usually cannot be well described with a single simple model because these structural parameters normally show various distributions instead of single values. According to the variation of numbers and positions of Ag nanoparticles on SiO_2 nanocarriers shown in Figures 4 and 7 and the higher experimental absorption around 300 nm as mentioned above, it is reasonable to consider the present SiO_2@Ag core−shell nanoparticles as a mixture of spherical Ag and SiO_2 nanoparticles. Then, the experimental spectrum of SiO_2@Ag can thus be fitted with the summation of the individual spectrum of Ag nanoparticles (calculated) and SiO_2 nanocarriers (experimental) with various fractions. The experimental spectrum of SiO_2 nanoparticles was directly used for the above fitting to reduce structural distribution errors that might occur in the theoretical SiO_2 model. As can be seen in Figure 9, the calculated spectra were consistent with the experimental spectra, indicating that this approach is applicable to the present system. The nanoparticle diameter retrieved from the calculation for specimens of 1, 3, and 5 nm (TEM) Ag nanoparticle is 1.32, 1.92, and 1.96 nm, respectively. This mismatch in particle diameter between TEM images and UV−vis spectra may result from various structural distributions such as size, shape, relative fraction, and position of Ag and SiO_2 in the present specimens.

A great number of theoretical and experimental studies have demonstrated that one or more capping layers consisting of different dielectric materials with various thickness would greatly change the SPR of the core materials in terms of peak position and fwhm. These capping-layer dependencies of the core SPR may be used to characterize the nature and layer thickness of the capping materials. In this sense, melamine was selected to be the target analyte for the liquid-type SiO_2@Ag core−shell nanoparticulate sensor for demonstration. Because the aqueous solution of melamine has almost no absorption in the range of 300−1100 nm, the absorption spectra for the melamine-capped SiO_2@Ag nanosensors are quite similar to that for pure SiO_2@Ag nanoparticles. A series of precise quantitative analyses of the Ag SPR peaks was then carried out for characterization of melamine response.

When the melamine solution was added to the cuvette, a clear red shift in the Ag SPR peak was observed. The plasmon shift as a function of melamine concentration is shown in Figure 9a. It is clearly evident that the change is quick for small concentrations of melamine and is increased with increasing

concentration of melamine. The mechanism underlying the sensing mechanism for Ag nanocrystal dispersions is intriguing. The large number of amine groups of melamine facilitates the covering of Ag nanoparticles. This may plausibly explain the role of melamine as a capping agent of the Ag nanoparticle dispersion, which can interact with amine groups of the melamine, forming Ag-NH_2. The SPR peak shift may then be a result of bond establishment between the silver and melamine. Simultaneously, it is clear that the larger silver nanoparticles exhibit a higher peak shift, as shown in Figure 9a, which further evidences more Ag-NH_2 bond formation.

The nonlinear tendencies for these three melamine capped SiO_2@Ag samples are very similar and seem to follow the Langmuir equation, which has become popular for describing solution−solid adsorption data and estimating adsorption equilibrium constants.[25] The Langmuir equation for nanoparticle system can be expressed as

$$N = \frac{N_{max} \cdot KC_{eq}}{1 + KC_{eq}}$$

where N represents the equilibrium sites of Ag nanoparticles capped by melamine and N_{max} is the maximum available sites of Ag nanoparticles for melamine. K is the adsorption equilibrium constant and C_{eq} is the equilibrium analyte concentration. For present experiments, N and N_{max} should be, respectively, transferred to$\Delta\lambda$ and$\Delta\lambda_{max}$ for numerical analysis. Here we simply assume that N is proportional to$\Delta\lambda$ and the C_{eq} can be replaced with the initial melamine concentration C_0 because of the relatively low concentration of Ag sites compared with the melamine concentration C_0. Then, the modified equation, which describes the SiO_2@Ag nanosensor response ($\Delta\lambda$) as a function of the melamine concentration, was directly applied to fit the experimental data. To obtain good mathematical fittings, as shown in Figure 10a, an extra constant term of 1.12, 1.92, and 1.72 nm was introduced for 1, 3, and 5 nm Ag specimen, respectively. The adsorption equilibrium constant K for 1, 3, and 5 nm Ag is 4.4×10^3, 2.4×10^3, and 8.8×10^3 M^{-1}, respectively.

The sensitivity η of the present Ag SPR sensors can be defined as

$$\eta = \frac{\Delta\lambda}{\Delta C}$$

where $\Delta\lambda$ and ΔC represent the SPR shift and the concentration change of melamine, respectively. The sensitivity derived from the differential plot of Figure 9a is given in Figure 9b, where a strong melamine concentration dependence of sensitivity can be clearly found for these three SiO_2@Ag nanosensors. The derivative peak intensity moves toward a lower value, whereas the size of Ag nanoparticles decreases along with the nanosensors. For the nanosensors with larger Ag nanoparticles distributed along the silica surface, the sensitivity can be as high as 10 ppb. The particle-size-dependent sensitivity is the same as the theoretical calculation from Slistan-Grijalva et al.[20] In addition, the peak position also suggests a suitable concentration range that can be well differentiated with the best resolution toward the melamine molecule. Although Roldán demonstrated excellent sensing properties of Ag nanoparticles that the FWHMs of Ag SPR greatly depend on the relative size of amine layer and the Ag core,[25] according to our experimental observations, the SPR peak shift shows better sensing features than

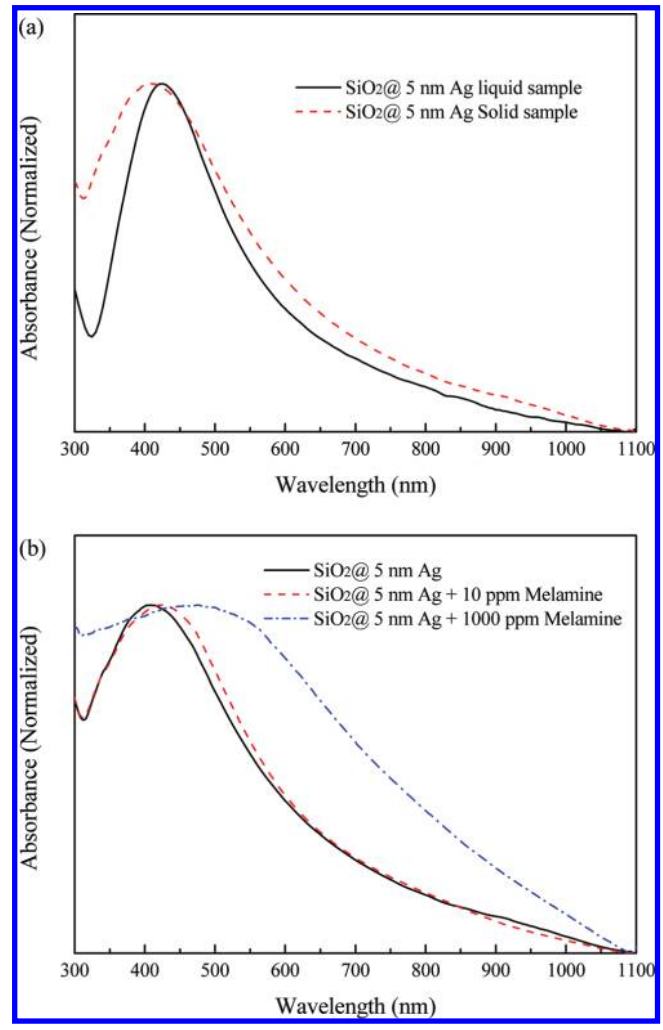

Figure 10. (a) Absorption spectra for the liquid-type 5 nm SiO_2@Ag nanocarriers and the solid-state 5 nm SiO_2@Ag nanosensor film on the optical glass substrate. (b) Absorption spectra for the solid-type film immerged in various concentrations of melamine.

FWHMs. Surely, for sensing characterization, the changes of SPR peak position and fwhm are correlated but the fwhm seems to be more easily affected by the size distribution of sensing nanoparticles, that is, Ag.

Spectral Behavior between Liquid-Type and Solid-Type SiO_2@Ag Nanosensors. However, because one alternative role of the SiO_2 matrix is acting as a spacer to separate effectively the deposited fine Ag nanoparticles from undesirable agglomeration as a result of attraction interactions, it is then more desirable to compare the SiO_2@Ag nanosensors either employed as a liquid-type sensor as illustrated in Figure 9 or employed as a solid-type sensor by forming a thin-film structure. Figure 10a demonstrates the resulting difference between the absorption spectra of the liquid-type 5 nm SiO_2@Ag nanosensors and the solid-type 5 nm SiO_2@Ag film on the optical glass substrate. The absorption band for the liquid- and solid-type nanosensors has been subtracted from the as-measured data. The SPR peak position for the SiO_2@Ag nanoparticle film shows a blue shift with an increase in fwhm compared with the liquid-based one. Similar tendency was visible for 1 and 3 nm. When SiO_2@Ag nanocarriers were deposited onto glass substrate to form a nanoparticle film, the local concentration of Ag nanoparticles may increase because of the dense packing of SiO_2@Ag nanocarriers. If the Ag nanoparticles are close enough to each other, then the coupling effect of the neighboring Ag nanopar-

ticles should play a dominant role in the resulting spectrum, although this is not the present case because of the very low Ag filling ratio. The only slight blue shift of SPR shown in Figure 10a suggests that the SiO_2 nanomatrix indeed played an important role as a spacer in well separating the ultrafine Ag nanoparticles from undesirable agglomeration, even when consolidating into a solid-type film, as a compared with that in suspension state. Besides, an extra test for a long-term storage (for 6 months at ambient environment) of the liquid-type nanosensor showed almost the same SPR spectra as those from initially prepared (not shown here), which further confirmed the role of SiO_2 spacer in stabilizing the Ag nanoparticles. (The influence of Ag oxidation has been considered but showed a negligible effect on the resulting spectral structure.)

It is expected that the spectral variation due to the interaction of melamine molecule on the SiO_2@Ag nanoparticle films is quite similar to that with a liquid-type sensor, as shown in Figure 10b, because the SiO_2 nanoparticles offer a nice separation for the extremely fine Ag nanoparticles, rendering a relatively stable spectral response in either form of entity. However, the sensitivity for melamine measurement is greatly enhanced, that is, the red shift is 18 nm for 10 ppm melamine in solid films compared with 7 nm in liquid-type sensor. A significant red shift for 1000 ppm is also detected in contrast with the liquid case. Although such a great shift and broadening may arise from not only the result of a simple melamine absorption on Ag nanoparticles but also the possible effect of a dense and thick rest melamine layers coated on films, this feature is still distinct enough for the present SiO_2@Ag nanocarriers for sensory applications.

4. Conclusions

Silver-decorated silica core−shell nanoparticles (namely, SiO_2@Ag nanospheres) were successfully synthesized by a facile and one-step process based on the modified Stöber method, with a silica core ~20 nm in diameter and a silver nanoparticles ranging from 1 to 5 nm in diameter. The sizes of silica and silver nanoparticles were well-controlled by fine-tuning of the pH value and reaction temperature of the diluting aqueous medium. The resulting SiO_2@Ag nanospheres were nicely employed as an optical sensor for melamine detection with an attainable resolution on the order of 10 ppb, and the sensitivity reached a maximal, which is silver-size-dependent, ranging from 0.1 to 1000 ppm, and the use of 5 nm silver nanoparticles appeared to show the best optical-responsive behavior toward the melamine molecules. The firmly attached, well-separated silver nanoparticles on the silica surface ensure an excellent optical stability and sensitivity and measuring reliability over the resulting optical behavior of the SiO_2@Ag nanospheres either in a liquid-type (as a suspension) or solid-type (as a thin film) structural configuration. The role of silica nanoparticles can then be well-defined as a colloidal stabilizer and a spacer for the spatial stabilization of the silver nanoparticles, ensuring a well-defined separation between the silver nanoparticles, either in the fluid form or consolidated form, with promising sensing capability.

References and Notes

(1) Kobayashi, Y.; Katakami, H.; Mine, E.; Nagao, D.; Konno, M.; Liz-Marzan, L. M. *J. Colloid Interface Sci.* **2005**, *283*, 392.
(2) Yin, Y.; Lu, Y.; Sun, Y.; Xia, Y. *Nano Lett.* **2002**, *2*, 427.
(3) Graf, C.; Vossen, D. L. J.; Imhof, A.; van Blaaderen, A. *Langmuir* **2003**, *19*, 6693.
(4) Serra, A.; Fillippo, E.; Re, M.; Palmisano, M.; Vittori-Antisari, M.; Buccolieri, A.; Manno, D. *Nanotechnology* **2009**, *20*, 165501.
(5) Lee, K. S.; El-Sayed, M. A. *J. Phys. Chem. B* **2006**, *110*, 19220.
(6) Xu, K.; Wang, J. X.; Kang, X. L.; Chen, J. F. *Mater. Lett.* **2009**, *63*, 31.
(7) Flores, J. C.; Torres, V.; Popa, M.; Crespo, D.; Calderon-Moreno, J. M. *J. Non-Cryst. Solids* **2008**, *354*, 5435.
(8) Liz-Marzán, L. M.; Giersig, M.; Mulvaney, P. *Langmuir* **1996**, *12*, 4329.
(9) Hache, F.; Ricard, D.; Flytzanis, C. *J. Opt. Soc. Am. B* **1986**, *3*, 1647.
(10) Jin, R.; Cao, Y. W.; Mirkin, C. A.; Kelly, K. L.; Schatz, G. C.; Zheng, J. G. *Science* **2001**, *294*, 1901.
(11) Sun, Y.; Mayers, B.; Xia, Y. *Nano Lett.* **2003**, *3*, 675.
(12) Cheng, W.; Wang, E. *J. Phys. Chem. B* **2004**, *198*, 24.
(13) Ai, K.; Liu, Y.; Lu, L. *J. Am. Chem. Soc.* **2009**, *132*, 9497.
(14) Wei, F.; Lam, R.; Cheng, S.; Lu, S.; Ho, D.; Li, N. *Appl. Phys. Lett.* **2010**, *96*, 133702.
(15) Han, C.; Li, H. *Analyst* **2010**, *135*, 583.
(16) Kalele, S. A.; Ashtaputre, S. S.; Hebalkar, N. Y.; Gosavi, S. W.; Deobagkar, D. N.; Deobagkar, D. D.; Kulkarni, S. K. *Chem. Phys. Lett.* **2005**, *404*, 136.
(17) Mishra, Y. K.; Mohapatra, S.; Kabiraj, D.; Mohanta, B.; Lalla, N. P.; Pivin, J. C.; Avasthi, D. K. *Scr. Mater.* **2007**, *56*, 629.
(18) Pellegrini, G.; Mattei, G.; Bello, V.; Mazzoldi, P. *Mater. Sci. Eng., C* **2007**, *27*, 1347–1350.
(19) Mie, G. *Ann. Phys.* **1908**, *25*, 377.
(20) Slistan-Grijalva, A.; Herrera-Urbina, R.; Rivas-Silva, J. F.; Ávalos-Borja, M.; Castillón-Barraza, F. F.; Posada-Amarillas, A. *Physica E* **2005**, *27*, 104.
(21) Bohren, C.; Huffman, D. *Absorption and Scattering of Light by Small Particles*; Wiley: New York, 1983.
(22) Zou, S. L.; Schatz, G. C. *Chem. Phys. Lett.* **2005**, *403*, 62.
(23) Hornyak, G. L.; Patrissi, C. J.; Martin, C. R. *J. Phys. Chem. B* **1997**, *101*, 1548.
(24) Homola, J. *Surface Plasmon Resonance Based Sensors*; Springer-Verlag: Berlin, 2006.
(25) Roldán, M. V.; Scaffardi, L. B.; de Sanctis, O.; Pellegri, N. *Mater. Chem. Phys.* **2008**, *112*, 984.

JP106185M